Epitaxial Synthesis, Band Offset, and Photoelectrochemical Properties of Cubic Ga$_2$S$_3$ Thin Films on GaAs (111) Substrates

H. F. Liu,[a,z] **K. K. Ansah Antwi,**[a] **C. S. Chua,**[a] **J. Huang,**[b] **S. J. Chua,**[a] **and D. Z. Chi**[a]

[a]*Institute of Materials Research and Engineering (IMRE), A*STAR (Agency for Science, Technology and Research), Singapore 117602, Singapore*
[b]*Department of Electrical and Computer Engineering, National University of Singapore, Singapore 117576, Singapore*

Uniform and crack-free cubic Ga$_2$S$_3$ thin films have been epitaxially synthesized on n-GaAs (111) substrates by sulfurization. Atomic-force microscopy revealed that the Ga$_2$S$_3$ surface is dominated by nanoparticles of smaller than 50 nm in diameter. The nanoparticles, clustered into regular triangle structures that hierarchically packaged on GaAs, significantly reduced the reflectance of GaAs. Low-temperature photoluminescence revealed typical acceptor-like defects while X-ray photoemission spectroscopy revealed type-I heterojunction with a valence-band offset of 0.6 eV for the Ga$_2$S$_3$/GaAs heterostructure. Photoelectrochemical properties of the Ga$_2$S$_3$/n-GaAs (111) heterojunction are studied and compared with those of bare n-GaAs (111) substrate in a typical three-electrode setup.

Because of their optimal band gaps (1.1 to 1.7 eV) for efficient solar driven water splitting, conventional semiconductors, including Si, GaAs, and GaP, have shown great promise in the direct photoelectrolysis of water to generate hydrogen fuel using sunlight.[1–3] Unfortunately, these semiconductors are generally unstable—either being corroded or passivated—when working as a photoanode in aqueous electrolytes.[4] Coating of metals and/or transparent metal oxides could somehow stabilize the semiconductor photoanode during water oxidation. Hu et al. recently reported that a thin amorphous TiO$_2$ layer of 4 to 143 nm in thickness coated on Si or GaAs by atomic layer deposition can effectively prevent their photocorrosion.[3] This TiO$_2$ coating, together with a layer of patterned Ni islands, stabilized the semiconductor photoanodes and promoted their efficiency for water oxidation.[3] Here, the benefit of TiO$_2$ coating is twofold, one is its larger bandgap than that of the semiconductors, so that the light absorption of the semiconductors is not much affected. The other is its electronic defects, which promote the electrical conduction of holes.

Gallium sulphide has long been of interest as a surface passivation material for GaAs. Recent studies revealed that Ga$_2$S$_3$ is highly resistive to light irradiation.[5] Intrinsically, Ga$_2$S$_3$ is rather hole conductive because the Ga sublattice of Ga$_2$S$_3$ is 1/3 unoccupied (i.e., Ga vacancies) which forms electron traps located at ∼0.4–0.7 eV above the valence-band maximum (VBM).[6,7] These characteristics of Ga$_2$S$_3$ as well as its large bandgap (>3.0 eV) are basically common with those of TiO$_2$ when coated on GaAs photoanode as mentioned above. Recently, we reported a simple and low-cost material growth method that yields Ga$_2$S$_3$ crystals on epiready n-type GaAs (111) substrates.[8] However, the crystal phase of the Ga$_2$S$_3$ layer varied from cubic to monoclinic and/or hexagonal along the growth direction; onset of film cracking and lift-off also occurred due to the large film thickness (∼450 nm).

In this work, thinner Ga$_2$S$_3$ layers were prepared in a tube-furnace system.[9] The detailed growth procedure for Ga$_2$S$_3$ can be found in Ref. 8, the only variations here are the reduced growth temperature and time, i.e., from 650°C and 20 min to 600°C and 10 min, respectively. The structural and optical properties of the Ga$_2$S$_3$ were characterized using atomic-force microscopy (AFM), high-resolution X-ray diffraction (HRXRD, $\lambda_{Cu-k\alpha1}$ = 0.1541 nm), temperature-dependent photoluminescence (PL). Both 532-nm (from a Nd:YAG laser) and 325-nm (from a He-Cd laser) excitations were employed in the PL studies. The band offset of the Ga$_2$S$_3$/GaAs heterostructure, which is hitherto unknown in the literature, was measured by using X-ray photoelectron spectroscopy (XPS).[10]

Photoelectrochemical properties of the Ga$_2$S$_3$ coated n-GaAs were studied with a typical three-electrode setup consisting of a Pt-foil

as the counter electrode, Ag/AgCl as the reference electrode, and Ga$_2$S$_3$/n-GaAs as the working electrode; 0.1 M Na$_2$SO$_4$ was used as the electrolyte. A solar simulator setting at AM1.5 (100 mW/cm^2) was used as the light source for the illumination. The illuminated area on the working electrode is about 1.0 cm^2. Gas evolution analysis was carried out in a gastight circulating system filled with argon (1.0 atm). A 1.0 V bias was applied across the coated film and the Pt electrode. A solar simulator, adjusted to a power density of 50 mW/cm^2, was used as the light source. The amount of gas evolved was determined through a gas chromatograph.

The image shown in Fig. 1a is taken by a nomarski microscope, which shows a uniform and crack-free surface of the obtained Ga$_2$S$_3$ layer. The microstructure of the Ga$_2$S$_3$ surface recorded by AFM is shown in Fig. 1b, where one sees that nanoparticles of smaller than 50 nm in diameter clustered into submicron regular triangle structures that hierarchically packaged on the GaAs substrate. The in-plane orientation of the individual triangle structures more or less aligned with one another. Optical spectroscopy studies (spectra not shown for the sake of brevity) revealed that the surface reflectance of the GaAs (111) substrate is significantly reduced by such a Ga$_2$S$_3$ coating, especially in the wavelength range from ultraviolet to visible. A typical cross-sectional scanning-electron microscopic (SEM) image is shown in Fig. 1c, from which the thickness of the Ga$_2$S$_3$ layer (i.e., 150 nm) is clearly determined. It is also seen that the Ga$_2$S$_3$ layer is uniform in thickness and the heterostructure has a sharp interface as indicated by the arrow.

Figure 2a shows the HRXRD θ/2θ-scan pattern collected from the Ga$_2$S$_3$/GaAs heterostructure around the (111) atomic planes, which, together with the ϕ-scan patterns collected from the (220) atomic planes in Fig. 2b, provides clear-cut evidence that the Ga$_2$S$_3$ is cubic phase and epitaxially grown on the GaAs substrate with the epitaxial relationship of [$\bar{1}$10]Ga$_2$S$_3$(111)//[$\bar{1}$10]GaAs(111). This epitaxial relationship, typically the 3-fold in-plane rotation symmetry [Fig. 2b], is consistent with the collective in-plane orientation of the triangle structures in Fig. 1b. Figure 2c shows a reciprocal space mapping (RSM) collected around the (220) atomic planes of both the Ga$_2$S$_3$ epilayer and the GaAs substrate. The RSM was collected in a skew configuration,[11] so that the alignment between the Ga$_2$S$_3$ (220) and GaAs (220) diffraction peaks in Qx does not necessary imply the absence of strain relaxation in the Ga$_2$S$_3$ epilayer. In fact, a careful calculation of the lattice spaces from Figs. 2a and 2c, using a_{GaAs} = 0.5653 nm as the reference, revealed d_{111} = 0.3005 nm and d_{220} = 0.1840 nm for the Ga$_2$S$_3$ epilayer. These results, when assuming a_{Ga2S3} = 0.5215 nm (JCPDS-ICDD 43-916), correspond to lattice strains of ε_{111} = −0.30% and ε_{220} = −0.28% remaining in the Ga$_2$S$_3$ epilayer. The relatively small lattice strains and the almost same strain in the ⟨111⟩ and ⟨220⟩ directions provide evidence that the Ga$_2$S$_3$

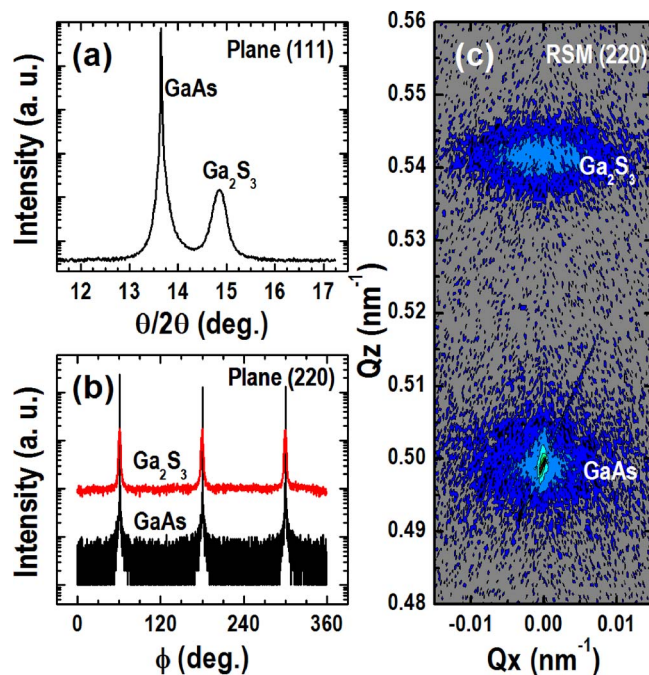[z]E-mail: liuhf@imre.a-star.edu.sg
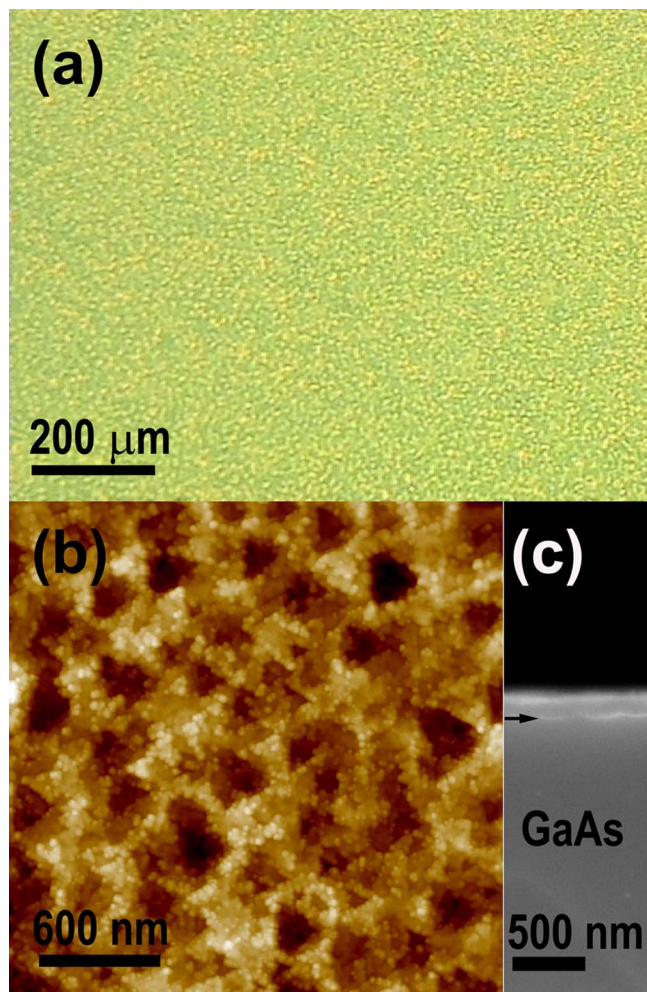
Figure 1. (a) surface image recorded by Nomarski microscopy from the Ga$_2$S$_3$ layer grown on a GaAs (111) substrate; (b) surface image recorded by AFM from the Ga$_2$S$_3$ layer grown on a GaAs (111) substrate; (c) cross-sectional SEM image recorded from the Ga$_2$S$_3$/GaAs (111) heterostructure, the arrow indicates the location of the Ga$_2$S$_3$/GaAs (111) interface.

Figure 2. HRXRD patterns collected from the Ga$_2$S$_3$/GaAs (111) heterostructure (a) in θ/2θ scan around the (111) atomic planes, (b) in φ scan around the (220) atomic planes. (c) Reciprocal space mapping (RSM) collected in a skew-configuration around the (220) atomic planes.

epilayer is nearly completely relaxed. Since the lattice mismatch between cubic Ga$_2$S$_3$ and GaAs is quite large (-7.75%), the nearly complete strain relaxation of the 150 nm thick layer without generating any film creaks is most likely due to the submicron structures that consisted of nanoparticles [Fig. 1b].

Figure 3a presents a typical PL spectrum collected from the Ga$_2$S$_3$/GaAs heterostructure at 10 K using a 532-nm laser excitation. Likewise, Fig. 3b presents the PL spectra collected at 10–180 K using a 325-nm laser excitation. The spectrum in Fig. 3a exhibits two dominant features corresponding to the near-bandedge emission (NBE) and a deep-level emission (DLE) of GaAs located at about 1.48 and 1.21 eV, respectively. This is because the excitation energy (2.33 eV) is much smaller than the bandgap energy of Ga$_2$S$_3$ (>3.0 eV). When a high-energy excitation is used, new features P$_1$-P$_4$ emerged at the higher energy side of the GaAs emissions [marked by asterisks in Fig. 3b]. These new emerged features can be attributed to the defect-related emissions (P$_1$-P$_3$) and the NBE (P$_4$) of the Ga$_2$S$_3$ epilayer. It is known that the 1/3 unoccupied Ga-sublattices in Ga$_2$S$_3$ form acceptor-like defects located at 0.4–0.7 eV above its VBM.[6–8] Transitions of excited electrons from the conduction-band and/or shallow donors to the Ga vacancies and/or their excited states give rise to the PL emissions of P$_1$-P$_3$.[12,13] A careful look at the defect-related PL emissions in Fig. 3b revealed that P$_1$ and P$_2$ have the similar intensity evolutions as a function of temperature; the decrease in intensity of

P$_3$ is much faster than those of P$_1$ and P$_2$. These comparisons indicate that there is a competition between the recombination channels of P$_1$/P$_2$ and P$_3$ when the sample temperature is varied, most likely due to the varied excitations of the Ga vacancies. The NBE feature of Ga$_2$S$_3$ [i.e., P$_4$ in Fig. 3b] indicates that the bandgap energy of the cubic Ga$_2$S$_3$ is $\sim$3.2 eV. This value is slightly larger than that obtained by optical absorption spectroscopy (3.0 eV) but closer to that obtained by PL (3.4 eV) in the literature.[8,12–15]

To our knowledge, the band offset of Ga$_2$S$_3$/GaAs heterostructures is lacking in the literature. Most of the reported studies on Ga$_2$S$_3$ were focused on bulk crystals for optical/optoelectronic applications and surface passivation of GaAs.[16–20] The former cases have nothing to do at all with the band offset while in the later cases the Ga$_2$S$_3$ layers are usually too thin (i.e., a few monolayers) for the band offset measurement. In this work, cubic Ga$_2$S$_3$ thin layers with quite good structural and optical properties have been epitaxially grown on GaAs (111) substrates. In this light, the VB offset of the Ga$_2$S$_3$/GaAs (111) heterostructure can be measured by XPS according to the band diagram shown in Fig. 4, where, the valence- and conduction-band offsets read

$$\Delta E_V = \left(E_{As3d}^{GaAs} - E_V^{GaAs} \right) - \left(E_{S2p}^{Ga_2S_3} - E_V^{Ga_2S_3} \right) + \left(E_{S2p}^{Ga_2S_3} - E_{As3d}^{GaAs} \right) \quad [1]$$

$$\Delta E_C = E_g^{Ga_2S_3} - E_g^{GaAs} - \Delta E_V \quad [2]$$

To verify the difference of $E_{S2p}^{Ga_2S_3} - E_{As3d}^{GaAs}$ in Eq. 1, a thin layer of Ga$_2$S$_3$ (<10 nm) was prepared on an n-GaAs (111) substrate so that the XPS signals can be detected from both the Ga$_2$S$_3$ layer (i.e., S2p) and the GaAs substrate (i.e., As3d).

Figures 5a–5c show the XPS spectra collected from a thick (150 nm) and a thin (<10 nm) Ga$_2$S$_3$-coated n-GaAs (111) heterostructures and a bare n-GaAs (111) substrate, respectively. Besides the typical VB and the core levels of S2p and As3d, there appears a peak at the lower binding energy side of As3d as indicated by the arrows in both Figs. 5b and 5c. The origin of this peak is unclear at this stage; nevertheless, according to Eq. 1, the binding energy alignment of As3d in Figs. 5b and 5c and that of S2p in Figs. 5a and 5b determine
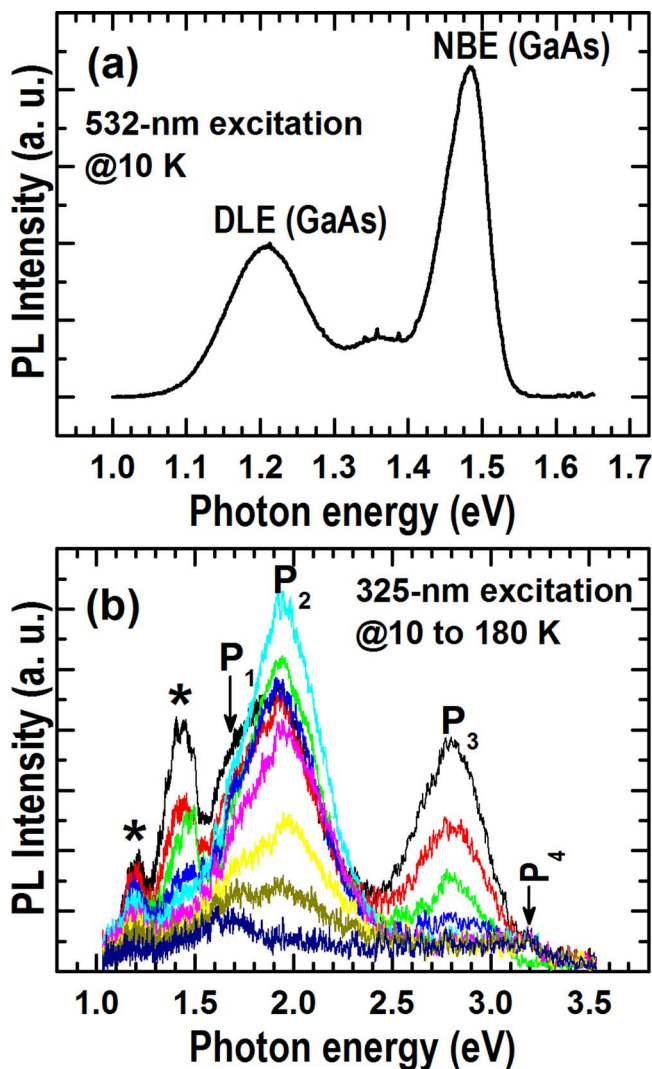
Figure 3. (a) PL spectrum collected at 10 K from the Ga_2S_3/GaAs (111) heterostructure using a 532-nm laser excitation, (b) temperature-dependent PL spectra collected from the Ga_2S_3/GaAs (111) heterostructure at 10–180 K using a 325-nm laser excitation. The asterisks indicate the emissions from GaAs.
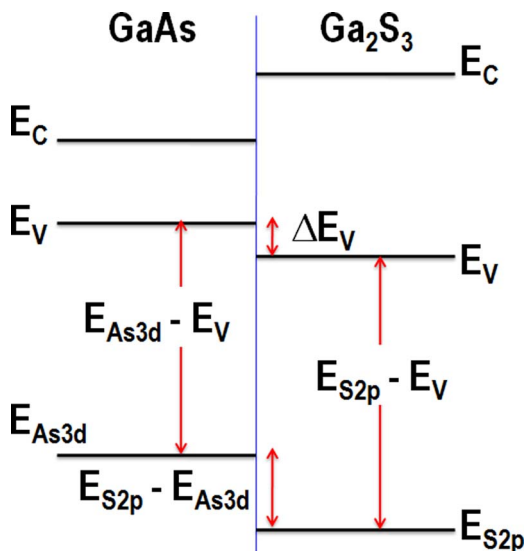
Figure 4. Schematic energy band diagram for the Ga_2S_3/GaAs heterostructure.
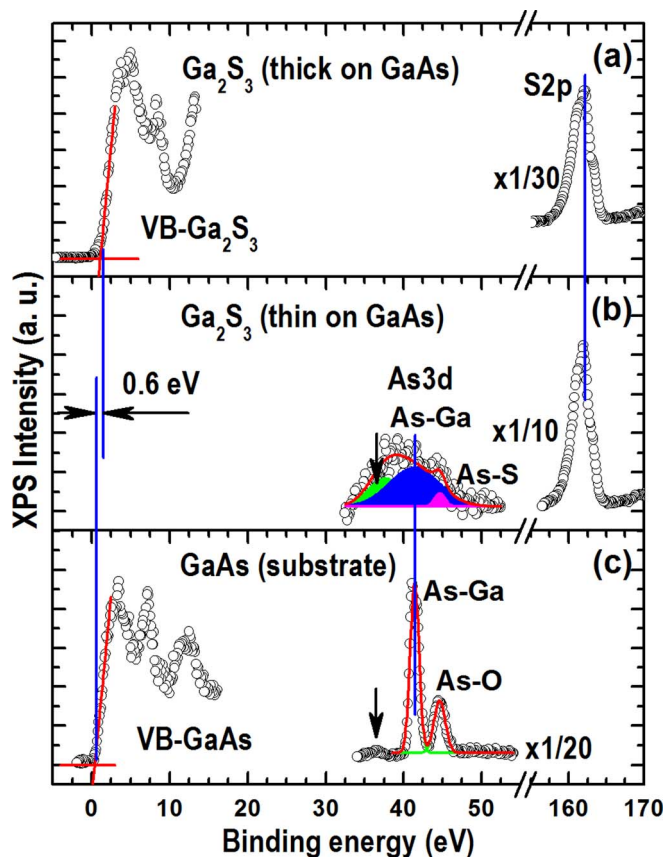
**Figure 5.** XPS spectra for the valance-band offset measurement of the Ga_2S_3/GaAs (111) heterostructure: (a) S2p and valence-band (VB) spectra of a thick (~150 nm) Ga_2S_3-on-GaAs (111) sample, (b) S2p and As3d spectra of a thin (<10 nm) Ga_2S_3-on-GaAs (111) sample, and (c) As3d and VB spectra of a bare GaAs (111) substrate.

the VB offset for the Ga_2S_3/GaAs (111) heterostructure, which is 0.6 eV with the VBM of Ga_2S_3 lower than that of GaAs. In consequence, the conduction-band offset, in terms of Eq. 2, is 1.18 eV, assuming that the bandgap energies of GaAs and Ga_2S_3 are 1.42 and 3.20 eV, respectively. It is thus obvious that a type-I heterojunction is formed in the epitaxial Ga_2S_3/GaAs (111) heterostructure.

Presented in Fig. 6a are the linear sweep voltammograms of the 150-nm Ga_2S_3-coated n-GaAs (111) photoanode in 0.1 M Na_2SO_4 electrolyte measured under dark and AM1.5 illuminations. For comparison, a bare n-GaAs (111) substrate is also measured under the same conditions and the results are presented in Fig. 6b. It is clearly seen that not only the photocurrent but also the dark current are significantly increased by the Ga_2S_3 coating. Based on the structural properties of the Ga_2S_3 coating discussed earlier, we believe that the increase in photocurrent is mainly caused by the reduced surface reflectance while the increase in dark current is due to the roughened surface that increased the effective surface reaction area (see later discussion). Also seen in Figs. 6a–6b is that the onset of the increase in the photocurrents is lowered from the potential of 0 to −0.45 V versus Ag/AgCl by the Ga_2S_3 coating. This potential lowering is reasonable since the VB offset of the Ga_2S_3/GaAs (111), as measured by XPS, is 0.6 eV.
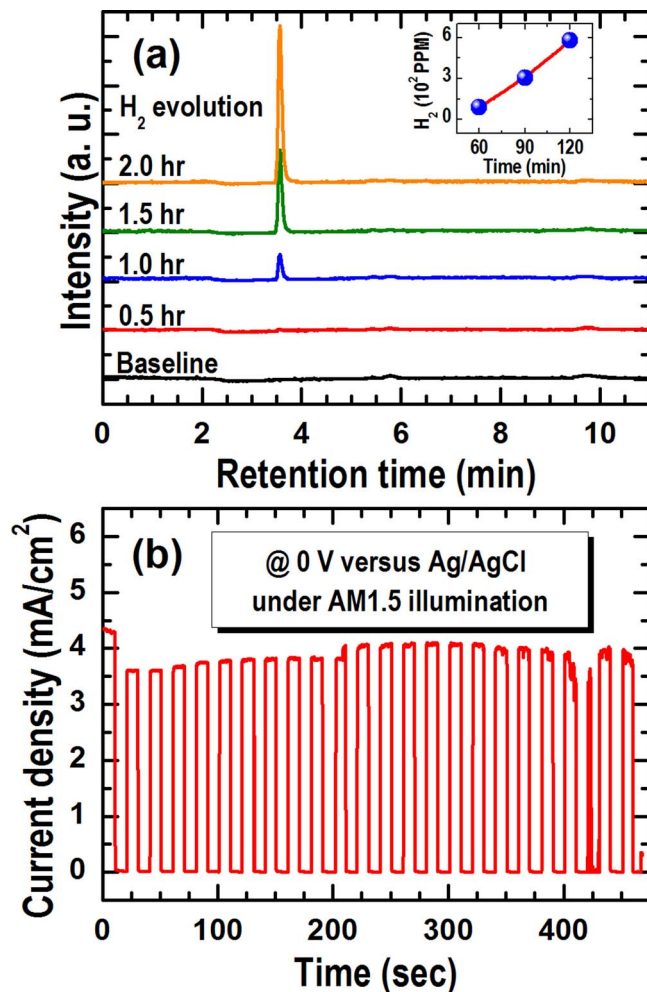
Hydrogen evolution reaction at the Pt counter electrode is further analysed. Figure 7a shows the H_2 evolution with Ga_2S_3/n-GaAs (111) as the photoanode, which was immersed in 0.1 M Na_2SO_4 electrolyte, biased at 1.0 V versus Ag/AgCl, and under an illumination of 50 mW/cm². Evolved H_2 gas was clearly detected after about a 1-hour reaction and the gas production [inset in Fig. 7a] nearly linearly increases with the reaction time. The undetectable H_2 at the initial stage
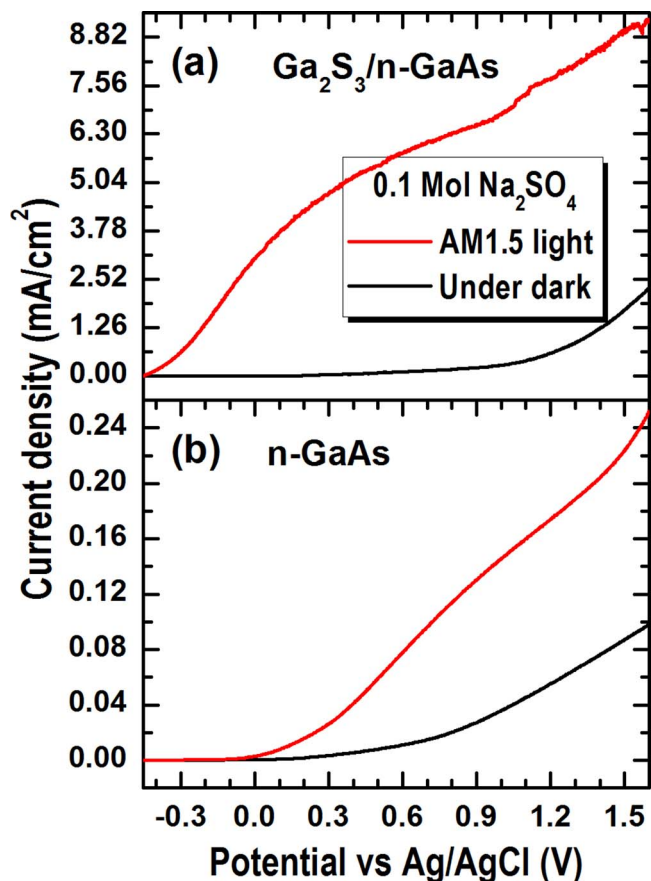
Figure 6. Linear sweep voltammograms of (a) Ga₂S₃/n-GaAs (111) and (b) n-GaAs (111). Measurements were carried out under dark and simulated solar illumination in 0.1 M Na₂SO₄ electrolyte.

Figure 7. (a) Hydrogen evolution as a function of time on the Pt counter electrode in 0.1 M Na₂SO₄ electrolyte; simulated solar adjusted to 50 mW/cm² was illuminated on the Ga₂S₃/n-GaAs (111) photoanode and the applied voltage was 1.0 V versus Ag/AgCl during the gas analysis. The inset shows the increase in the concentration of hydrogen with the reaction time. (b) Photocurrent of the Ga₂S₃/n-GaAs (111) photoanode biased at 0 V versus Ag/AgCl under chopped solar illumination of AM1.5 (100 mW/cm²).

of reaction could be attributed to the system stabilization (e.g., gas dilution in the chamber) and/or the limitation of the detector. Figure 7b shows the photocurrent profile under chopped-illumination and biased at 0 V versus Ag/AgCl, which provides evidence for the stable photocurrent at the initial stage of gas evolution reactions. It has to be noted that the oxygen evolution is too weak for quantitative analysis. Morphology evolutions (SEM images not shown) after the two-hour testing revealed that the reaction on the Ga₂S₃/GaAs photoanode is dominated by photocorrosions of Ga₂S₃. The large amount of Ga vacancies in Ga₂S₃, having the defect levels located at 0.4–0.7 eV above its VBM,[6–8] can compensate the VB offset and lead to the hole transfers freely from GaAs to Ga₂S₃. Electrocatalyst, for example, those of patterned Ni islands introduced by Hu et al.[3] onto the surface of amorphous TiO₂ coated on Si or the ultrathin Ni overlayers on GaAs, can be used to enhance the oxygen evolution on the surface of Ga₂S₃/GaAs photoanode, which, however, is still in progress.

In conclusion, cubic Ga₂S₃ layers have been epitaxially grown on n-GaAs (111) substrates by sulfurization. The epitaxial relationship, [1̄10]Ga₂S₃(111)//[1̄10]GaAs(111), has been determined by HRXRD, which is consistent with the collective in-plane orientation of the surface triangle structures of Ga₂S₃. The submicron triangle structures, clustered by nanoparticles of smaller than 50 nm in diameters, significantly reduced the reflectance of GaAs. Although the lattice mismatch between cubic Ga₂S₃ and GaAs is quite large, the Ga₂S₃ layer, nearly completely relaxed in the crystal lattices, is crack-free and exhibits a mirror-like surface. A valence-band offset of 0.6 eV has been measured by XPS for the Ga₂S₃/GaAs (111) heterostructure. Such a Ga₂S₃ layer, coated on n-GaAs (111) substrates, significantly enhanced the photocurrent when working as a photoanode. This effect has been attributed to the largely reduced surface reflectance as well

as to the increased surface reaction/corrosion area. Although the hydrogen evolution on the counter electrode is apparent and stable after the system stabilization for about 1 hour, the oxygen evolution on the working electrode is very weak due to the lack of electrocatalyst.

References

1. O. Khaselev and J. A. Turner, *Science*, **280**, 425 (1998).
2. C. R. Cox, M. T. Winkler, J. J. H. Pijpers, T. Buonassisi, and D. G. Nocera, *Energy Environ. Sci.*, **6**, 532 (2013).
3. S. Hu, M. R. Shaner, J. A. Beardslee, M. Lichterman, B. S. Brunschwig, and N. S. Lewis, *Science*, **344**, 1005 (2014).
4. M. G. Walter, E. L. Warren, J. R. McKone, S. W. Boettcher, Q. Mi, E. A. Santori, and N. S. Lewis, *Chem. Rev.*, **110**, 6446 (2010).
5. M. Zhang, X. Jiang, L. Zhou, and G. Guo, *J. Mater. Chem. C*, **1**, 4754 (2013).
6. I. M. Askerov, A. O. Mekhrabov, C. K. Aslanov, B. G. Tagiev, and S. M. Nakhmetov, *Phys. Stat. Sol. (a)*, **105**, K151 (1988).
7. M. Guymont, A. Tomas, M.-P. Pardo, and M. Guittard, *Phys. Stat. Sol. (a)*, **113**, K5 (1989).

8. H. F. Liu, K. K. Ansah Antwi, N. L. Yakovlev, H. R. Tan, L. T. Ong, S. J. Chua, and D. Z. Chi, *ACS Appl. Mater. Interfaces*, **6**, 3501 (2014).
9. H. F. Liu, K. K. Ansah Antwi, S. J. Chua, and D. Z. Chi, *Nanoscale*, **6**, 624 (2014).
10. H. F. Liu, G. X. Hu, H. Gong, K. Y. Zang, and S. J. Chua, *J. Vac. Sci. Technol. A*, **26**, 1462 (2008).
11. This is a symmetric configuration with the incident and diffracted x-ray beams having the same angle from the surface plane while the surface normal is tilted away from the beam plane formed by the incident and diffracted beams.
12. T. Aono and K. Kase, *Solid State Commun.* **81**, 303 (1992).
13. T. Aono and K. Kase, *Solid State Commun.* **83**, 749 (1992).
14. H. Chen, *Crystal Growth and Optical Properties of Ga$_2$S$_3$* (Thesis, National Taiwan University of Science and Technology, 2013).

15. V. P. Mushinskii, L. I. Palaki, and V. V. Chebotaru, *Phys. Stat. Sol. (b)*, **83**, K149 (1977).
16. H. A. Ei. Shaikh, M. Abdal-Rahman, A. E. Belal, and I. M. Ashraf, *J. Phys. D: Appl. Phys.*, **29**, 466 (1996).
17. C. Yoon, F. D. Medina, L. Martinez, T. Park, M. Jin, and W. Kim, *Appl. Phys. Lett.*, **83**, 1947 (2003).
18. A. Tomas, M. Guymont, M. P. Pardo, M. Guittard, and J. Flahaut, *Phys. Stat. Solidi A*, **107**, 775 (1988).
19. H. Chiu, Y. Huang, L. Chang, and F. Chien, *Semicond. Sci. Technol.*, **23**, 035029 (2008).
20. N. Barbouth, Y. Berthier, J. Oudar, J.-M. Moison, and M. Bensoussan, *J. Electrochem. Soc.: Solid-State Sci. Technol.*, 1663 (Aug. 1986).